Glycobiology, 2021, vol. 31, no. 1, 29–43
doi: 10.1093/glycob/cwaa046
Advance Access Publication Date: 29 May 2020
Original Article

OXFORD

Cancer Biology

4-Methylumbelliferone as a potent and selective antitumor drug on a glioblastoma model

Matías A Pibuel[1,2], Mariángeles Díaz[3], Yamila Molinari[4], Daniela Poodts[2], Lucas Silvestroff[4], Silvina L Lompardía[2,†], Paula Franco[4,†], and Silvia E Hajos[2]

[2]Departamento de Microbiología, Inmunología, Biotecnología y Genética, Facultad de Farmacia y Bioquímica, Instituto de Estudios de la Inmunidad Humoral (IDEHU)—CONICET, [3]Instituto de Estudios de la Inmunidad Humoral (IDEHU)—CONICET, and [4]Departamento de Química Biológica, Cátedra de Química Biológica Patológica, Facultad de Farmacia y Bioquímica, Instituto de Química y Fisicoquímica Biológicas (IQUIFIB)—CONICET, Universidad de Buenos Aires, Junin 956, C1113 CABA, Argentina

[1]To whom correspondence should be addressed: Tel: +54 11 52874406/07; Fax: +54 11 4964 2400; email: pibuelmatias@gmail.com

[†]Silvina L Lompardía and Paula Franco contributed equally to the realization of this work.

Received 19 March 2020; Revised 19 May 2020; Editorial Decision 19 May 2020; Accepted 19 May 2020

Abstract

Glioblastoma (GBM), the most frequent primary tumor of the central nervous system, has a median survival of 14.6 months. 4-Methylumbelliferone (4MU) is a coumarin derivative widely used as a hyaluronan synthesis inhibitor with proven antitumor activity and without toxic effects reported. We aim to evaluate the antitumor effect of 4MU alone or combined with temozolomide (TMZ) on a GBM cell line, its absence of toxicity on brain cells and its selectivity for tumor cells. The antitumor effect of 4MU alone or combined with TMZ was evaluated on GL26 cells by assessing metabolic activity using the XTT assay, cell proliferation by BrdU incorporation assay, migration by the wound healing assay, cell death by fluorescein diacetate/propidium iodide (FDA/PI) staining, apoptosis by membrane asymmetry and DNA fragmentation and metalloproteinase activity by zymography. The levels of hyaluronan and its capacity to counteract the effects of 4MU and the expression of RHAMM and CD44 were also determined. The toxicity and selectivity of 4MU were determined by XTT assay and PI staining on normal brain primary cell culture (NBPC-GFP) and GL26/NBPC-GFP cocultures. The GL26 cells expressed RHAMM but not CD44 and synthesized hyaluronan. 4MU decreased hyaluronan synthesis, diminished proliferation and induced apoptosis, while reducing cell migration and the activity of metalloproteinases, which was restored by addition of hyaluronic acid. Furthermore, 4MU sensitized GL26 cells to the TMZ effect and showed selective toxicity on tumor cells without exhibiting neurotoxic effects. We demonstrated for the first time the cytotoxic effect of 4MU on GBM cells, highlighting its potential usefulness to improve GBM treatment.

Key words: 4-Methylumbelliferone, glioblastoma, hyaluronan, temozolomide, toxicity

Introduction

Glioblastoma (GBM), also known as IV grade glioma, is the most frequent primary tumor of the central nervous system (CNS). This malignancy shows a fast-growing behavior, presenting a high mortality rate. The tissue invasive capacity is a key factor for GBM progression (Louis et al., 2016). Although the therapeutic strategies to treat cancer have improved over the last years, few therapeutic options are available for high-grade gliomas, particularly, for GBM. The standard treatment strategy for GBM includes surgical resection of the tumor followed by radiotherapy and treatment with the first-line drug temozolomide (TMZ) (Anton et al., 2012). However, GBM has a very poor prognosis, with a median survival of 14.6 months (Anjum et al., 2017). As for the treatment with TMZ, not only does drug resistance occur—in roughly 50% of patients—but also myelosuppression and hepatotoxicity are observed (Anjum et al., 2017; Houy and Le Grand, 2018; Sasmita et al., 2018).

Even though aggressiveness and resistance phenomena are attributed to the activity of malignant cells, the extracellular matrix (ECM) surrounding the tumor also plays an important role in drug penetration, invasion and modulation and evasion of the immune system. The brain ECM can be divided into two major groups: the one belonging to the parenchyma and that of the vessel's basement membrane. Hyaluronic acid (HA) is the central component of the parenchymal ECM to which proteins and proteoglycans adhere forming a tridimensional net (Ferrer et al., 2018). HA is a linear nonsulfated glycosaminoglycan (GAG), consisting of repetitive units of D-glucuronic acid and N-acetyl-D-glucosamine (Auvinen et al., 2013; Boregowda et al., 2006; Provenzano and Hingorani, 2013; Toole, 2004). HA is involved in several physiological functions, such as the maintenance of tissue architecture, wound healing, leukocyte trafficking and growth and cell differentiation (Joy et al., 2018; Khaldoyanidi et al., 2014; Termeer et al., 2003). Moreover, HA plays a key role in neural stem cell niches, where is involved in the generation, proliferation and maturation of neural stem/progenitor cells during the CNS development and repair (Preston and Sherman, 2011; Su et al., 2019).

The quality and quantity of this GAG are finely regulated. This control occurs majorly during its synthesis by HA synthases (HAS) and its degradation mediated by hyaluronidases (Hyals). Other key point in HA metabolism is the cell internalization trough membrane hyalderins, as CD44 and RHAMM that which are the most relevant HA receptors in oncology (Csoka and Stern, 2013; Hascall et al., 2014; Jiang et al., 2011). The development of several malignancies is known to be featured by deregulation of HA metabolism. An increase of HA above physiological levels has been associated with induction of cell proliferation, migration, inhibition of apoptosis and development of multidrug resistance (Sironen et al., 2011; Toole, 2004, 2009). In patients with GBM, higher HA levels have been found in the tumor stroma, as compared to the surrounding normal tissue. These HA levels also correlated with tumor grade (Delpech et al., 1993). Furthermore, in GBM in vitro models, HA has proved to promote proliferation, migration and invasion (Park et al., 2008). It can thus be speculated that reducing HA levels would constitute a promising antitumor strategy.

The coumarin derivative 4-methylumbelliferone (4MU) has been widely used as an inhibitor of HA synthesis. 4MU binds to glucuronic acid to prevent the formation of UDP-glucuronic acid, the HAS substrate and it has been shown that it generates a diminish of both HAS-2 and HAS-3 mRNA levels (Kakizaki et al., 2004; Kultti et al., 2009). Even more, the UDP-glucuronyltransferases (UGT) generate 4-Methylumbelliferyl glucuronide (4MU-G), which contributes to hyaluronan synthesis inhibition (Nagy et al., 2019). Furthermore, there are reports showing CD44 and RHAMM modulation mediated by 4MU (Cho et al., 2017; Lokeshwar et al., 2010). However, the mechanisms of its anticancer effect remain still unclear. Notably, 4MU has no effect on coagulation; more importantly no adverse effects were observed over a wide range of doses in several clinical trials. Even more, in Europe and Asia, 4MU has been approved for use in humans as a choleretic and antispasmodic agent (Nagy et al., 2015).

Although the effect of 4MU on GBM has not been assessed, antiproliferative, proapoptotic and antimetastatic effects have been demonstrated on several carcinoma and sarcoma in vivo and in vitro models (Arai et al., 2011; Lokeshwar et al., 2010; Nagy et al., 2015; Piccioni et al., 2012; Urakawa et al., 2012; Vigetti et al., 2011).

We have previously demonstrated the antineoplastic effects of 4MU on human chronic myeloid leukemia cell lines. In that model, 4MU sensitized these cells to the action of imatinib and vincristine (Lompardía et al., 2013, 2017). Besides, we demonstrated that the supplementation with HA does not totally abrogate the antitumor effects of 4MU, suggesting the existence of mechanisms that are independent of HA synthesis inhibition. According to that, it has recently been suggested that 4MU modulates the activity of metalloproteinases (MMPs) in a HA-independent fashion (Ishizuka et al., 2016; Karalis et al., 2019). Therefore, we consider that the mechanisms of 4MU independent of hyaluronan synthesis inhibition might be very important in its antitumor effect.

Besides their primary role in ECM remodeling, MMPs, which are Zn-dependent endopeptidases, regulate different processes such as migration, proliferation, apoptosis, angiogenesis, immune responses and tumor development through the mobilization of growth factors and the release of cytokine/chemokine transporters or inhibitors (Chaudhary et al., 2016; Chintala et al., 1999). The role of MMPs in GBM progression has also been demonstrated (Chintala et al., 1999; Musumeci et al., 2015; Nakada et al., 2003; Zheng et al., 2017). In fact, MMP-2 and MMP-9 mRNAs are significantly augmented in GBM, as compared to the normal brain, and MMP-9 is thought to play a role in the CD44-mediated GBM cell migration (Chetty et al., 2012; Varga et al., 2010).

We hypothesized that 4MU could be an effective and selective drug for the treatment of GBM. This study aimed to evaluate the antitumor effect of 4MU, both alone and in combination with TMZ, on a GL26 murine GBM cell line. The cytotoxicity and selectivity of 4MU were also evaluated on a murine normal brain cells and on a GL26/NBPC-GFP coculture, respectively.

In this work, we have demonstrated for the first time that 4MU decreases cell viability, MMP activity and migration while increased the levels of apoptosis on a GBM model. As expected, HA enhanced cell migration but it could only prevent the effect of 4MU on metalloproteinase activity. Furthermore, 4MU sensitized GL26 cells to TMZ treatment by enhancing the effect of TMZ on cell death. Finally, we found that 4MU treatment had low toxicity on normal brain cells in culture and showed a selective effect on tumoral cells when GL26 and NBPC were treated in coculture. The results presented in this work highlight the potential usefulness of 4MU, either alone or in combination with TMZ, to improve the effectiveness of GBM treatment.

Results

4MU reduces HA synthesis and decreases cell viability of GL26 cells by inducing apoptosis

Considering that 4MU inhibits HA synthesis, we first studied this inhibition on GL26 cells by ELISA and Immunofluorescence. We found that GL26 cells were able to synthesize HA (765.7 ± 31.48 ng/mL/10^5 cells), while 4MU partially decreased its production in a dose-dependent manner after 24 h of treatment. In accordance, such reduction was also observed by IFI (Figure 1A).

To assess the antitumor effect of 4MU, we then studied cell viability by the XTT assay. GL26 cells were treated with increasing doses of 4MU for 48 h. The formazan product generated by living cells was measured spectrophotometrically at 450 nm. Figure 1B shows that 4MU decreased the metabolic activity of GL26 cells in a dose-dependent manner, with this reduction being significant at doses of 4MU higher than 125 µM. Similar results were observed on human GBM cell lines (Supplementary Figure 1).

Taking into account that 4MU abrogated the metabolic activity on GL26 cells, we decided to evaluate if this reduction was due to an inhibition of cell proliferation. As shown in the Figure 1C, after 48 h of treatment with 4MU, the cell proliferation was inhibited in a dose-dependent manner.

Additionally, cell death was studied using fluorescein diacetate/propidium iodide (FDA/PI) staining and flow cytometry. After 72 h of treatment with 4MU the percentage of PI-positive cells increased in a dose-dependent manner. This increase was statistically significant for 4MU doses over 250 µM (Figure 1D). Similar results were observed at 48 h, while 4MU failed to modify the proportion of PI-positive cells at 24 h (Supplementary Figure 2).

Apoptosis was then evaluated by flow cytometry by annexin-V-PE staining (Figure 1E). A significant induction of apoptosis in GL26 cells was observed at 72 h with 4MU doses above 250 µM. It is noteworthy that at 1000 µM, 4MU induced apoptosis in more than 80% of GL26 cells. Finally, the results obtained with annexin-V-PE staining were supported by evaluation of the GL26 nuclear integrity with DAPI staining. The percentage of cells showing DNA fragmentation was increased after 48 h of treatment with 4MU. However, differences were statistically significant only at 1000 µM 4MU (Figure 1F). These results suggest that 4MU inhibits metabolic activity through a cytostatic and cytotoxic effect by decreasing cell viability and inducing apoptosis in GL26 cells. Moreover, and taking into account that 4MU partially reduced the HA levels, it is possible that part of the 4MU effects might be independent of HA inhibition.

4MU abrogates the migration of GL26 cells and MMP-2 activity

Another issue of interest was the evaluation of two processes closely related to the aggressiveness of GBM: cell migration and MMPs activity. For this purpose, the wound closure test and gelatin gel zymography were performed, respectively. As shown in Figure 2A, 4MU reduced wound closure at 18 h. Similar results were obtained after 6 and 24 h of treatment with 4MU (data not shown). Similarly, 4MU reduced MMP-2 activity (pro-MMP-2 or latent form) at 24 h, identified by comparing the position of bands with the molecular weight marker (Figure 2B). In both experiments, the effects of 4MU were dose-dependent. These results indicate that 4MU decreases GL26 cell migration and MMP-2 activity prior to inhibition of cell proliferation and cell death induction.

Both high molecular weight (HMW)-HA and low molecular weight (LMW)-HA enhance GL26 migration without affecting cell viability

First, the expression of CD44 and RHAMM was evaluated. As it is shown in Figure 3A, the GL26 cells showed high expression of RHAMM, but they did not express CD44.

Since HA induced cell migration and proliferation in other GBM models, we decided to study the effects of this GAG on metabolic activity, cell death, cell migration and MMP-2 activity on GL26 cells. The addition of neither LMW-HA nor HMW-HA affected the metabolic activity of GL26 cells (Figure 3B). To verify that cell viability was not influenced by HA, we evaluated cell death using the highest doses of HA. As a result, neither the percentage of PI-positive GL26 cells (Figure 3C) nor DNA fragmentation were affected by HA (Figure 3D). However, both HMW-HA (Figure 3E) and LMW-HA (Figure 3F) increased the wound closure index. Considering the dose that showed the greatest effect on cell migration, we performed zymography assays using 300 µg/mL of HA. Nevertheless, HA at this dose did not affect MMP-2 activity (Figure 3G).

All these results indicate that GL26 cells express RHAMM but not CD44 and that HA has no effect on cell viability while enhances migration without affecting MMP-2 activity of GL26 cells.

HA abrogates the effect of 4MU only on MMP-2 activity

Taking into account that the effects exerted by 4MU are associated with the inhibition of HA synthesis and that in our model the reduction of HA levels was verified, we evaluated if 4MU effects depend on the decrement of HA levels on GL26 cells. For this purpose, cells were cotreated with 4MU and HA and metabolic activity, cell death and migration, as well as MMP-2 activity were evaluated.

Our results demonstrated that neither HMW-HA (Figure 4A) nor LMW-HA (Figure 4B) were able to counteract the effect of 4MU on the metabolic activity of GL26 cells. Similarly, neither the percentage of cells with nuclear fragmentation (data not shown) nor that of PI-positive cells (Figure 4C) were affected after the HA and 4MU cotreatment. Although HA did not abrogate the effect of 4MU on the wound closure index (Figure 4D), it successfully counteracted the reduction generated by 4MU on MMP-2 activity, restoring the baseline levels (Figure 4E). These results suggest that the effect of 4MU on metabolic activity, cell death and migration would be independent of the inhibition of HA synthesis, while the effect of 4MU on MMP-2 activity would be dependent on that mechanism. Taking this into account, we consider that the mechanisms of 4MU independent of hyaluronan synthesis inhibition might be very important in its antitumor effect.

4MU present higher cytotoxic effect than TMZ on GL26

Considering that TMZ is the first line drug for GBM therapy, we compared the effects of 4MU and TMZ on the metabolic activity and death of GL26 cells.

As shown in Figure 5A, no significant differences were observed in metabolic activity between 4MU and TMZ treatments. However, the dose-response curves showed that 4MU has an IC50 lower than TMZ: 281.6 and 463.4, respectively ($P < 0.05$). Besides, no differences were observed in the percentages of PI-positive cells after treatment with 4MU or TMZ (Figure 5B). Furthermore, while it was observed that TMZ induces a higher percentage of annexin-V-PE positive cells than 4MU at 250 µM (reaching about 40% and 30%, respectively), at 1000 µM 4MU induces a greater percentage of

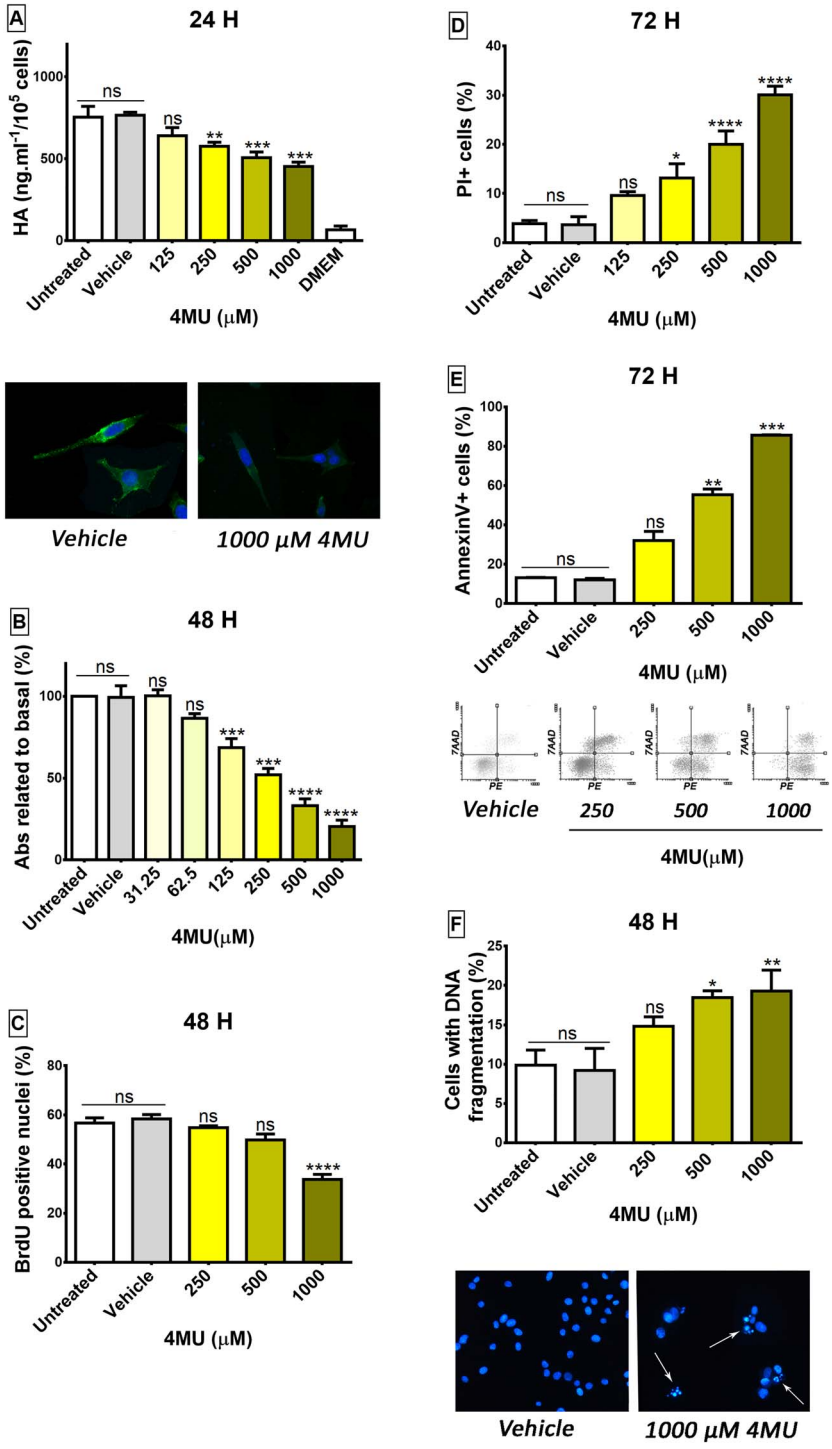

Fig. 1. Effect of 4MU on hyaluronan synthesis, viability and cell death. (**A**) Levels of HA in culture supernatant were evaluated by ELISA after treatment with 4MU for 24 h using the bHABP and avidin–HRP detection system. Values are expressed as HA concentration (ng/ml/105 cells). For IFI assay, cells were treated for 24 h with 4MU and then incubated with bHABP and revealed using streptavidin-cy2. Representative photographs of the HA immunofluorescence are shown below the graph. (**B**) GL26 cells were treated with 4MU for 48 h. The metabolic activity was then evaluated by the XTT assay. Results are expressed as the percentage of Abs in relation to untreated condition, as described in Material and Methods section. (**C**) Cell proliferation was determined by BrdU incorporation assay and immunofluorescence after 48 h of treatment. (**D**) Cell death was evaluated by FC using FDA/PI stain after treatment with 4MU for 72 h. The FDA stain was used as viability control. Bars represent the percentage of PI-positive cells. (**E**, **F**) The GL26 cell line was treated with 4MU for 72 h and apoptosis was then evaluated by FC using annexin-V/7AAD staining (**E**), and by nuclear fragmentation through DAPI staining (**F**). Values are expressed as the percentage of annexin-V-positive cells and cells with nuclear fragmentation, respectively. Representative FC dot plots and DAPI staining are shown under each bar graph. Arrows show fragmented nuclei in treated cells. Data are expressed as the mean ± SEM of at least three independent experiments. Asterisks represent statistical significance with respect to cells treated with vehicle: *$P < 0.05$, **$P < 0.01$, ***$P < 0.001$, ****$P < 0.0001$ and ns = nonsignificant difference. In all the assays at least one of the differences between doses is statistically significant ($P < 0.05$).

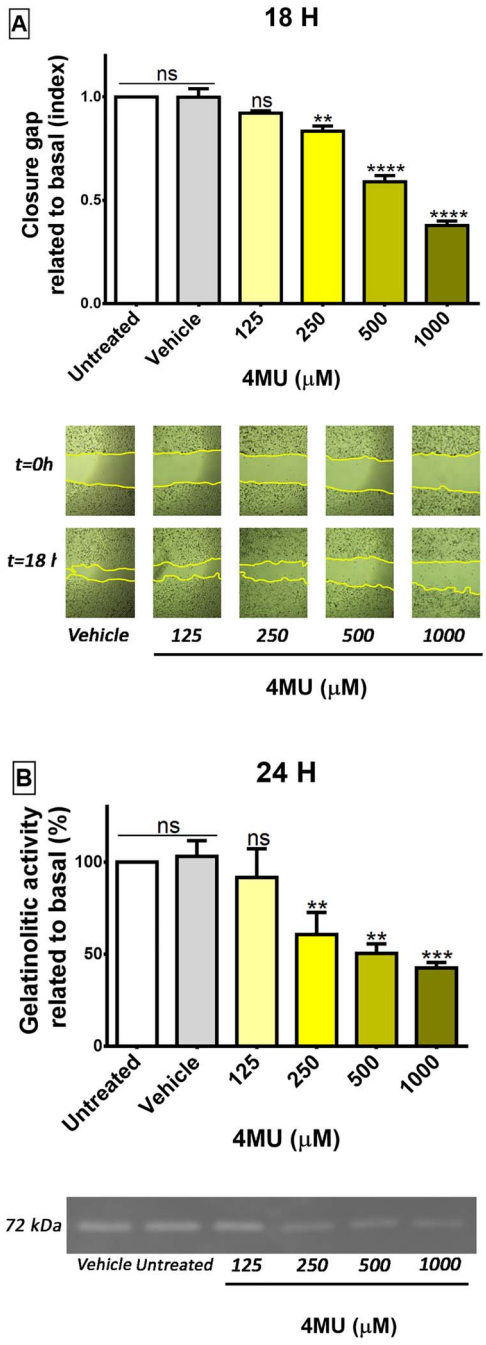

Fig. 2. Evaluation of cell migration and MMP activity. (**A**) GL26 cells were treated with 4MU and cell migration was then determined by the wound healing assay after 18 h. The same wound area was photographed at 0 and 18 h. Results were expressed as closure gap index calculated as described in Materials and Methods section. Representative photographs are shown below the graph. Yellow lines show the edges of migrating cells at 0 and 18 h. (**B**) GL26 cells were treated for 24 h and then, the MMP activity was determined by zymography. A representative photograph is shown below the graph. The band appears at ~72 kDa and corresponds to pro-MMP-2. Densitometric values were expressed in relation to untreated control cells and data were expressed as the mean ± SEM of at least three independent experiments. Asterisks represent statistical significance with respect to cells treated with vehicle: **$P < 0.01$, ***$P < 0.001$, ****$P < 0.0001$ and ns = non-significant difference. In both assays at least one of the differences between doses is statistically significant ($P < 0.05$).

annexin-V-PE positive cells than TMZ (85% vs. 70% respectively) (Figure 5C). These results suggest that 4MU at high doses presents a greater cytotoxic effect than TMZ on GL26 cells, both on the decrease of metabolic activity and in the induction of apoptosis.

The combination of 4MU and TMZ enhances GL26 cell death

Considering that 4MU and TMZ have different mechanisms of action, we tested the cytotoxic effect of the cotreatment with 4MU and TMZ in order to determine if both drugs together could improve the antitumor effects of each drug individually. We found that the cotreatment with 4MU and TMZ for 72 h, induced a significant increase in the percentage of PI-positive cells (Figure 6A) and, largely, in the percentage of annexin-V-PE-positive cells (Figure 6B) with respect to each drug alone. However, after 48 h of treatment, the combination of drugs did not modify the metabolic activity of GL26 cells, as compared to each drug alone (Supplementary Figure 3). Finally, Figure 6C shows that the combination of 4MU and TMZ had a synergistic effect at cell death level since all the combination indexes (CI) were less than 0.95. These results show that 4MU sensitized GL26 cells to the effect of TMZ. Therefore, the combination of 4MU and TMZ could be used to improve the GBM treatment.

4MU treatment has very low toxicity on normal brain cells

Antitumor drugs should exhibit a potent activity on cancer cells and a minimal toxicity on normal cells. To assess the neurotoxic effects of 4MU, NBPC cells obtained from wild type and actin::GFP transgenic animals were treated with different doses of 4MU and the metabolic activity, as well as the effects on cell death were then determined.

A minimal toxic activity was found for 4MU on NBPC-GFP causing only a 10% reduction in the metabolic activity after 48 h of treatment with 1000 μM 4MU (Figure 7A). Furthermore, the treatment with 4MU did not induce cell death, since it did not modify the percentage of PI-positive cells (Figure 7B) nor the number of cells with DNA fragmentation (Figure 7C). NBPC-GFP was indistinguishable from wild type NBPC, since similar results were obtained with cell cultures from both mice strains (data not shown). Even more, to confirm the low toxicity of 4MU on normal brain cells, we performed a XTT assay on normal stem cell neurospheres which have a high rate of proliferation. As is shown in Figure 7D, 4MU decreased the metabolic activity of neurospheres by about 15% only at the highest dose. These results indicate that 4MU presents very low toxicity on normal brain cells.

4MU shows a selective cytotoxic effect on GL26 cells without affecting normal brain cells in GL26/NBPC-GFP cocultures

Taking into account that 4MU showed antitumor effects on GL26 cells without showing cytotoxicity on NBPC-GFP, we studied the selectivity of this drug on GL26/NBPC-GFP cocultures. For this purpose, cocultures were treated with 4MU and after 72 h cell death was evaluated by PI staining. In this assay, viable NBPC-GFP cells showed a GFP single staining while dead NBPC-GFP cells showed GFP-PI double staining. On the other hand, viable GL26 cells were unstained while dead GL26 cells were stained only with PI. It is noteworthy that the mean GFP fluorescence intensity was diminished in the dead NBPC-GFP cell population, but was differentiated from GL26

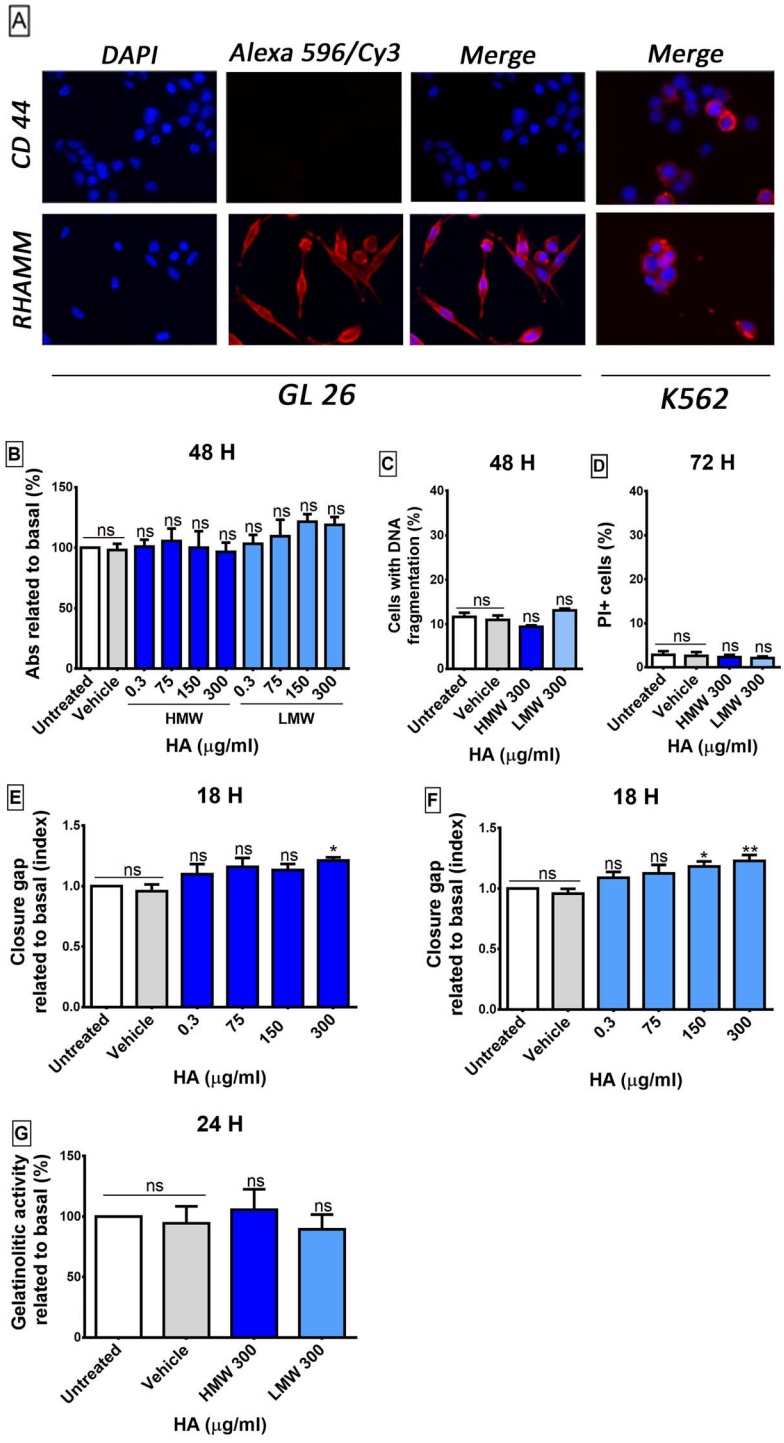

Fig. 3. Effect of HA on GL26 cell viability, cell death, MMP activity and cell migration. (**A**) The expression of RHAMM and CD44 was determined on GL26 by IFI. The k562 leukemia cell line was used as a positive control. (**B**) GL26 cells were treated with either HMW-HA or LMW-HA. The metabolic activity was then determined by the XTT assay after 48 h. Results are expressed as the percentage of Abs in relation to untreated control cells as described in Material and Methods section. (**C**) DNA fragmentation was analyzed by DAPI staining after 48 h of treatment. Data are expressed as the percentage of GL26 cells with nuclear fragmentation. (**D**) Cell death was evaluated by FDA/PI staining after 72 h of treatment. Data are expressed as the percentage of PI-positive cells. (**E**, **F**) GL26 cells were treated with either HMW-HA (**E**) or LMW-HA (**F**) and cell migration was determined by the wound healing assay after 18 h of treatment. The same wound area was photographed at 0 and 18 h. (**G**) MMPs activity of GL26 cells after 24 h of treatment determined by zymography. The gelatinolytic activity was calculated as the percentage of densitometry values of bands in relation to untreated control cells. Results are expressed as the closure gap index calculated as described in Material and Methods section. In all graphs, bars represent means ± SEM of at least five independent experiments. Asterisks represent statistical significance in relation to cells treated with vehicle: $^{*}P < 0.05$ and $^{**}P < 0.01$, ns = nonsignificant ($P > 0.05$).

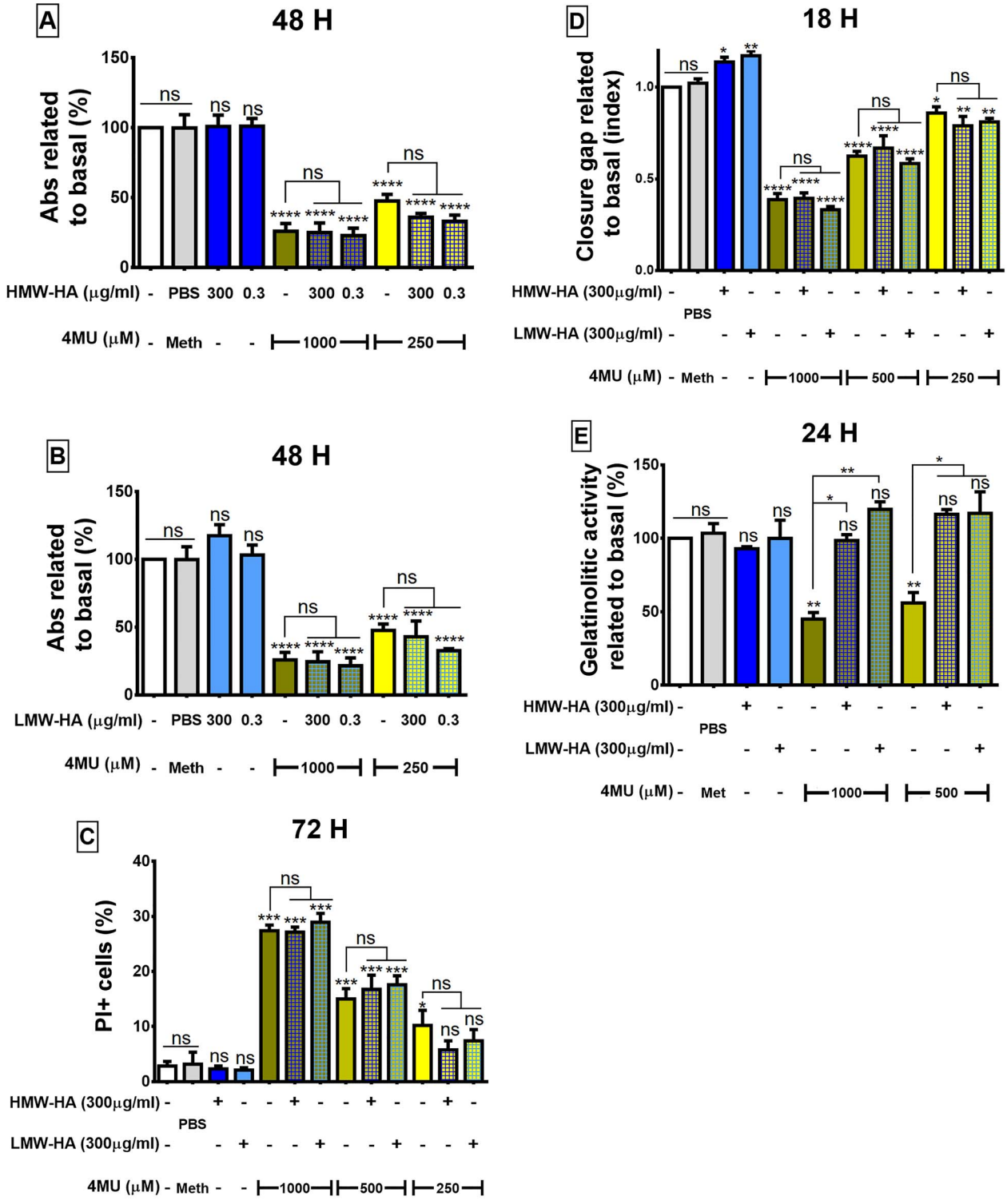

Fig. 4. Effects of the cotreatment with 4MU and HA on GL26 cells. (**A**, **B**) GL26 cells were treated with either HMW-HA (**A**) or LMW-HA (**B**) combined with 4MU.The metabolic activity was then determined by the XTT assay after 48 h of treatment. Results are expressed as the percentage of Abs in relation to untreated control cells as described in Material and Methods section. (**C**) GL26 cells were treated with either HMW-HA or LMW-HA combined with 4MU for 72 h. Cell death was then evaluated by FC using FDA/IP staining. Values are expressed as percentage of PI-positive cells. (**D**) Cell migration was determined by the wound healing assay after 18 h of treatment with either HMW-HA or LMW-HA combined with 4MU. Results are expressed as closure gap index in relation to untreated control cells as described in Material and Methods section. (**E**) The MMP activity was analyzed by zymography after 24 h of cotreatment of 4MU with either HMW-HA or LMW-HA. Bars represent means ± SEM of at least five independent experiments. Asterisks over bars indicate statistical significance in relation to cells treated with vehicle. $^{*}P < 0.05$, $^{**}P < 0.01$, $^{***}P < 0.001$, $^{****}P < 0.0001$ and ns = nonsignificant ($P > 0.05$). The same symbols over lines indicate differences between the indicated treatments.

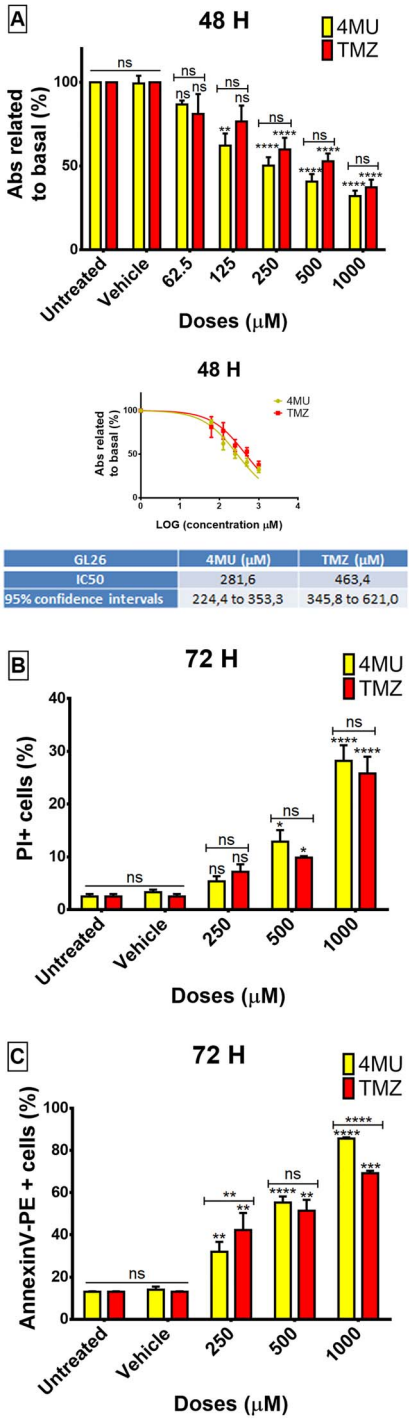

GL26	4MU (μM)	TMZ (μM)
IC50	281,6	463,4
95% confidence intervals	224,4 to 353,3	345,8 to 621,0

Fig. 5. Comparison between the effects of 4MU and TMZ on GL26 cells. (**A**) GL26 cells were treated with either 4MU or TMZ for 48 h and the XTT assay was then performed. The metabolic activity was expressed as the percentage of Abs in relation to untreated condition as described in Material and Methods section. The dose-response curves were obtained allowing the comparison of the IC50. (**B**, **C**) Cell death and apoptosis were evaluated by FC after 72 h of treatment with either 4MU or TMZ. FDA/PI (**B**) and annexin-V/7AAD (**C**) staining were performed. Values are expressed as percentages of PI-positive cells and annexin-V-positive cells, respectively. Bars represent the mean ± SEM of at least three independent experiments. Asterisks over bars indicate differences treated vs. cells treated with vehicle, *P < 0.05, **P < 0.01, ***P < 0.001 ****P < 0.0001 and ns = nonsignificant (P > 0.05). The same symbols over lines indicate differences between the indicated treatments.

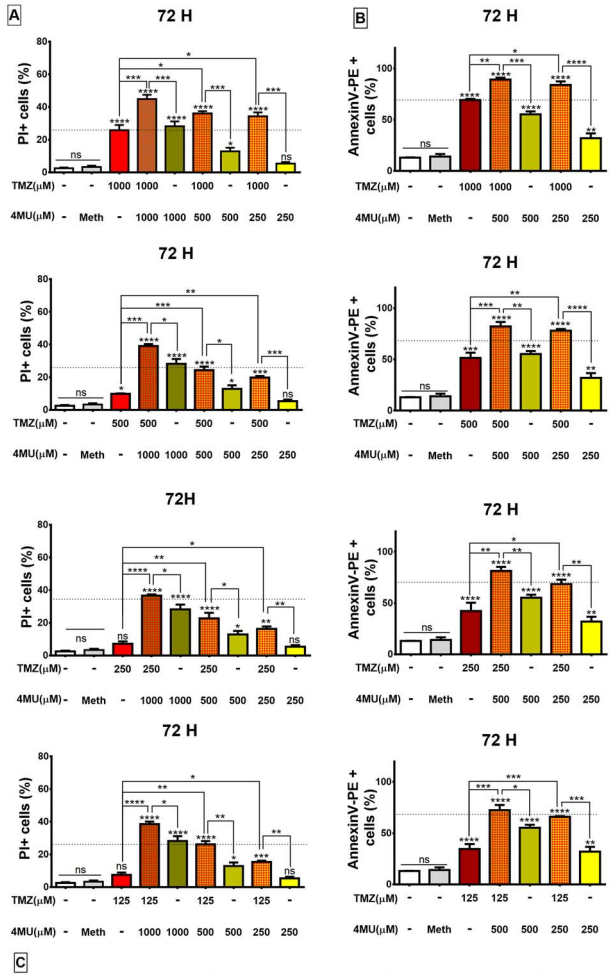

C

IP+ cells (where 0 ≤ efect ≤ 1)		125 μM TMZ	4MU + TMZ obtained result	250 μM TMZ	4MU + TMZ obtained result	500 μM TMZ	4MU + TMZ obtained result	1000 μM TMZ	4MU + TMZ obtained result
250 μM	Expected additive efect	0,124	0,154	0,122	0,163	0,147	0,198	0,298	0,344
4MU	Combination Index	0,809	Synergism	0,748	Synergism	0,741	Synergism	0,868	Synergism
500 μM	Expected additive efect	0,194	0,262	0,191	0,227	0,215	0,244	0,354	0,361
4MU	Combination Index	0,741	Synergism	0,843	Synergism	0,882	Synergism	0,980	Additive
1000 μM	Expected additive efect	0,336	0,386	0,334	0,367	0,353	0,391	0,467	0,449
4MU	Combination Index	0,871	Synergism	0,910	Synergism	0,903	Synergism	1,042	Additive

Fig. 6. Effects of the combined treatment with 4MU and TMZ on GL26 cell death. (**A**) GL26 cells were treated with either 4MU, TMZ or their combinations for 72 h. Cell death was then evaluated by FC using FDA/PI staining. Values are expressed as percentage of PI-positive cells. (**B**) GL26 cells were treated with 4MU, TMZ or their combination for 72 h and then apoptosis was evaluated by FC using annexin-V/7AAD staining. Results are expressed as percentage of annexin-V-positive cells. Bars represent the mean ± SEM of at least three independent experiments. Asterisks over bars indicate differences between treated vs. cells treated with vehicle, *P < 0.05, **P < 0.01, ***P < 0.001 ****P < 0.0001 and ns = nonsignificant (P > 0.05). The same symbols over lines indicate differences between the indicated treatments. The dotted lines in the graphs represent the percentages obtained with the highest dose of TMZ for each assay. (**C**) In respect to cell death, the effect of 4MU and TMZ combination was analyzed by effect-based strategy using the Bliss independence model, and the CI was calculated. Expected additive effect = (4MU effect + TMZ effect - 4MU effect x TMZ effect) x 100 (where 0 ≤ 4MU effect ≤ 1 and 0 ≤ TMZ effect ≤ 1). The resulting CI was calculated as: CI = (4MU effect + TMZ effect - 4MU effect x TMZ effect)/Combination effect (where 0 ≤ 4MU effect ≤ 1; 0 ≤ TMZ effect ≤ 1 and 0 ≤ Combination effect ≤ 1), being CI < 1 synergism, CI = 1 additive and CI > 1 antagonism with significant at the 5% level.

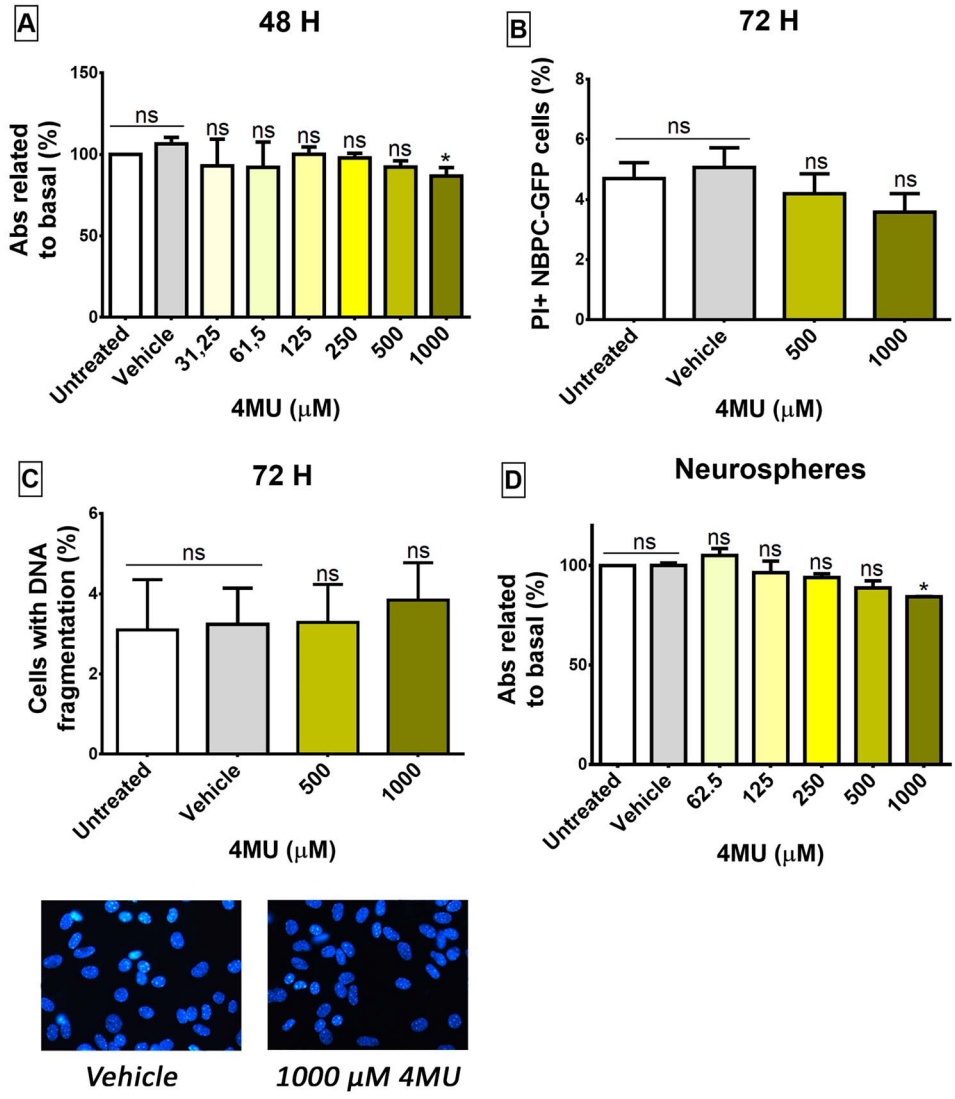

Fig. 7. Evaluation of 4MU toxicity on normal brain cells. (**A**) NBPC-GFP were treated with increasing concentrations of 4MU for 48 h and the metabolic activity was then determined. Results were expressed as the percentage of Abs in relation to untreated control cells as described in Material and Methods section. (**B**) Cell death was assessed by FC using PI staining. Results are expressed as percentage of PI-positive cells. A representative dot plot of the FC analysis is depicted on the right. (**C**) DNA fragmentation was analyzed by fluorescence microscopy by DAPI staining. (**D**) Neurospheres were treated with 4MU for 48 h and the metabolic activity was then determined. Results were expressed as the percentage of Abs in relation to untreated control cells, as described in Material and Methods section. Bars represent the percentage of cells with nuclear fragmentation. A representative immunofluorescence image is shown below the graph. Bars represent mean ± SEM of at least three independent experiments. Asterisks over bars indicate statistical difference in relation to cells treated with vehicle *$P < 0.05$, and ns = nonsignificant ($P > 0.05$).

dead cells, which displayed a much lower green autofluorescence intensity. These characteristics served to distinguish cell populations and allowed to analyze flow cytometry assays. 4MU induced a significant increase in the percentage of PI-positive GL26 cells, decreasing the number of viable GL26 cells. As a consequence, the proportion of viable NBPC-GFP cells augmented while the percentage of dead NBPC-GFP cells remained unchanged, as compared to cells treated with vehicle (Figure 8A).

In order to confirm these results, an immunofluorescence assay was performed on GL26/NBPC-GFP cocultures.

GL26 cells were identified by high expression levels of vimentin (Supplementary Figure 4), while GFP served as a marker for normal brain cells (Figure 8B). In these experiments, 4MU treatment did not affect the number of brain GFP-positive cells. In contrast, 4MU caused a great dose-dependent reduction in the number of vimentin-positive GL26 cells adhered to NBPC-GFP monolayer.

Discussion

GBM is a highly aggressive malignancy due to its fast-growing rate and its capacity to invade surrounding tissues. In this work, we studied for the first time the therapeutic potential of 4MU on the GL26 GBM cell line. We demonstrated that 4MU significantly reduced both hyaluronan synthesis and the metabolic activity of GL26 cells, inducing cell death in a dose-dependent manner. Furthermore, 4MU

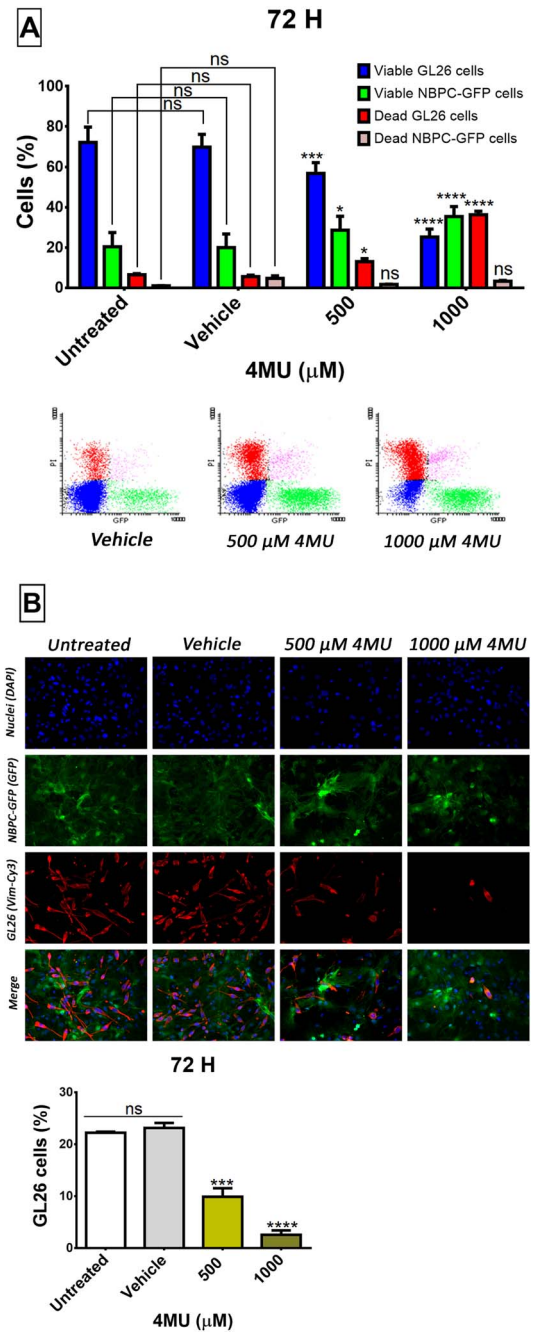

Fig. 8. Selectivity of 4MU for tumor cells in GL26/NBPC-GFP cocultures. GL26 cells were seeded onto a NBPC-GFP monolayer and incubated for 24 h. Then, the cocultures were treated with 4MU for 72 h. (**A**) Cell death was evaluated by FC using PI staining. Viable NBPC-GFP cells showed a GFP single staining while dead NBPC-GFP cells showed GFP-PI double staining. Viable GL26 cells were unstained while dead GL26 cells were only stained with PI. The GFP mean fluorescence intensity was diminished in dead NBPC-GFP cells population but they differentiated from GL26 dead cells, which displayed a lower green autofluorescence intensity. Results were expressed as the percentages of each population with respect to the total cell number. Representative dot plots are shown at right graphic. (**B**) Using immunofluorescence, NBPC-GFP and GL26 cells were identified as GFP-positive and vimentin-Cy3-positive cells, respectively. Results were expressed as the percentage of GL26 cells attached to the monolayer with respect to the total cell number. Bars represent means ± SEM of at least three independent experiments. Asterisks indicate statistical significance with respect to cells treated with vehicle, *$P < 0.05$, **$P < 0.01$, ***$P < 0.001$, ****$P < 0.0001$ and ns = nonsignificant ($P > 0.05$).

inhibited two processes closely related to this pathology, i.e. cell migration and MMP-2 activity. In accordance with these findings, we have previously shown that 4MU inhibited proliferation and induced senescence on myeloid leukemia cell lines (Lompardía et al., 2013). Moreover, other authors have described similar effects of 4MU in different tumor cells, suggesting the use of 4MU as a potential therapeutic alternative for hepatic, bladder and breast cancers as well as other malignancies (Karalis et al., 2019; Morera et al., 2017; Nagy et al., 2015; Piccioni et al., 2012).

4MU has been widely used as an inhibitor of HA synthesis (Nagy et al., 2015). Moreover, in our model, the coumarin derivative decreased HA synthesis in a dose-dependent manner. As HA is the main component of the parenchymal ECM of the CNS, and since it is a key regulator of tumor establishment and development, it is tempting to speculate that the effects of 4MU would be mediated by the reduction of HA synthesis. However, we found that the addition of HA to 4MU-treated cells only abrogated the inhibitory effect of 4MU on the activity of MMP-2. Other 4MU effects, such as the reduction of the cell metabolic activity, the induction of cell death, and the inhibition of cell migration, were not counteracted by the addition of HA. These findings indicate that most of the toxic effects of 4MU in GL26 cells seem to be mediated by mechanisms that are independent of the inhibition of HA synthesis. It is also possible that the addition of exogenous HA was not enough to counterbalance the HA deficit in 4MU-treated cells. The fact that HA is organized in a three-dimensional structure in the ECM suggests a complex scenario that is difficult to reproduce in vitro by the exogenous addition of soluble HA. More studies are required to corroborate this hypothesis. Yet, over the last years, some authors have also described HA-independent effects for 4MU toxicity (Ishizuka et al., 2016; Karalis et al., 2019). Similarly, we have previously shown that the 4MU-mediated inhibition of proliferation on chronic myeloid leukemia cell lines is only partially prevented by HA supplementation (Lompardía et al., 2013).

HA seems to be a promising target to achieve a potentially effective therapy for GBM. Several strategies have previously been proposed for diminishing the aggressiveness of GBM, including the blockade of HA interaction with its receptors, its degradation, the inhibition of intracellular HA-activated pathways and the inhibition of its synthesis (DeSouza et al., 2013; Tsatas et al., 2002).

In this work, we showed that both HMW-HA and LMW-HA enhance GL26 cell migration, which is in accordance with some studies that highlight the role of HA in cell migration and invasion of other glioma cells (DeSouza et al., 2013; Jin et al., 2009; Park et al., 2008). However, we did not find induction of MPP-2 activity after the treatment with neither HMW-HA nor LMW-HA. This finding indicates that both HMW-HA and LMW-HA would promote GL26 cell migration in an MMP-2-independent fashion. Although MMPs are known to favor cell migration (Chetty et al., 2012; Nakada et al., 2003; Zheng et al., 2017), in the context of brain ECM, particularly rich in HA, MMPs activity would be more related to neo-angiogenesis or vessel invasion, than cell migration (Chintala et al., 1999; Kast and Halatsch, 2012). Furthermore, multiple factors might be involved in GBM cell migration and in this environment, the activity of Hyals might be relevant (Ferrer et al., 2018; Junker et al., 2003; Novak et al., 1999). In addition, through their receptors, CD44 and RHAMM, GBM cells can easily interact with the hyaluronan of the brain ECM. In this work, we found that GL26 cells showed high expression of RHAMM, which is strongly related to HA-mediated cell migration (Maxwell et al., 2008), but did not express CD44. CD44 was implicated in HA-mediated cell proliferation, MMPs

activity and cell survival (Chetty et al., 2012; Mooney et al., 2016; Varga et al., 2010). These findings could partially explain the fact that HA only increased cell migration on GL26 cells without affecting other processes evaluated.

Combined drug therapies are a valuable alternative for the treatment of cancer not only because they allow the use of lower drug doses reducing adverse effects but also because they diminish the probability of drug resistance phenomena. The antitumor effect of 4MU was compared to that of TMZ, the first-line drug for the treatment of GBM. We showed that the GL26 cell line is sensitive to TMZ, even at low doses. These findings are in accordance with previous reports which demonstrated that GL26 cells do not express O6-methylguanine-DNA methyltransferase, which has been associated with TMZ resistance (Park et al., 2015). We found that 4MU exhibited a minor IC50 respect to TMZ on the metabolic activity of GL26 cells. Both drugs induced a similar degree of cell death, as assessed by PI staining; however, a differential behavior was observed when apoptosis was analyzed by the annexin-V assay. Higher cell death percentages were obtained with TMZ than 4MU at low doses, whereas at high doses the effect of 4MU was greater than the effect of the first line drug. It is noteworthy that TMZ is known to exert hepatotoxic and myelosuppressive effects in humans, while 4MU is a safe and well-tolerated oral medication, as indicated by clinical experience (Anjum et al., 2017; Houy and Le Grand, 2018; Nagy et al., 2015; Sasmita et al., 2018).

The combination of 4MU and TMZ exerted stronger effects than each drug alone at all the concentrations tested. The treatment with both drugs simultaneously promoted higher levels of GL26 cell death. These findings show that 4MU produces a great sensitization of GL26 cells to the first-line drug TMZ. In addition, the synergistic effect showed for the cotreatment is very interesting, since the combination of both drugs would contribute to cell death through different mechanisms of action, which might improve the GBM therapy. Accordingly, we have previously demonstrated that 4MU sensitized LMC cell lines to imatinib and vincristine, which are widely used to treat leukemia (Lompardía et al., 2013, 2017). Similar results were obtained by other authors with isofuranodiene, ADI-PEG20, aspirin and other drugs combined with TMZ on GBM cells (Brunetti et al., 2019; Navone et al., 2018; Przystal et al., 2018).

Any antitumor treatment should be highly toxic to tumor cells without affecting normal tissues. Although no adverse effects have been reported for 4MU, at the date the direct impact on brain cells remains unknown. In this work, we assayed for the first time the in vitro toxicity of 4MU on brain cells revealing that 4MU did not induce cell death at any of the concentrations tested on brain primary cultures as well as it exhibited very low toxicity on neural stem cells. Moreover, we developed a coculture design, in which GL26 cells were grown on a brain cell monolayer. On the GL26/NBPC-GFP coculture, 4MU showed a selective effect for tumor cells, inducing GL26 cells death without affecting normal brain cells. The effectiveness of the treatment with 4MU in a context in which tumor cells are intermingled with normal cells supports 4MU as an excellent nontoxic candidate for GBM therapy.

In this work, we demonstrated for the first time the antitumor effects of 4MU on a GBM model. 4MU has also proved to exert only mild toxic effects on normal brain cells. Moreover, we have shown that 4MU sensitizes GL26 cells to the first-line drug TMZ. Considering the results obtained herein, we conclude that 4MU alone or in combination with TMZ could be used to improve the effectiveness of the GBM treatment.

Materials and methods

Reagents

Recombinant HMW (1.5–1.8 × 10^6 Da) and LMW (CPN spol.s.r.o Czech Republic) HA were supplied by Farmatrade (Argentina). 4MU, biotinylated Hyaluronic Acid Binding Protein (bHABP), PI, FDA, 4′,6-diamidino-2-phenylindole (DAPI), gelatin, bisbenzimide 33258 (Höechst), glucose, BSA, XTT and phenazine methosulfate (PMS) were purchased from Sigma-Aldrich (USA). DMEM, L-glutamine, streptomycin and penicillin were purchased from Invitrogen (Argentina). The Annexin-V-PE Apoptosis Detection Kit I was purchased from BD Pharmingen™ (BD Bioscience, USA). TMZ was supplied by LKM laboratories (Argentina). The anti-CD44 monoclonal antibody was from IM7 clone (ATCC). The V9 antivimentin monoclonal antibody was from Santa Cruz Biotechnology (USA), the rabbit anti-Sox10 monoclonal antibody and the rabbit anti-RHAMM polyclonal antibody were purchased from Abcam Inc. (USA), the goat anti-PFGFRα monoclonal antibody was from Neuromics Antibodies (Edina, USA), and the mouse anti-Myelin basic protein (MBP) was from BioLegend Inc. (San Diego, USA). The goat antimouse cy3 and the goat cy3 anti rat secondary antibodies were from Jackson Immunoresearch (USA), the donkey anti rabbit Alexa 594 was from Molecular Probes (USA) and Mowiol (Calbiochem) was purchased from Merck S.A. (Argentina).

GL26 cell line cultures

The GL26 mouse GBM cell line (gently provided by Dr. M. Candolffi) was grown in adherent cultures at 37°C in a 5% CO_2 atmosphere with DMEM supplemented with 10% heat inactivated fetal bovine serum (FBS), 2 mM L-glutamine, 100 µg/mL streptomycin and 100 IU/mL penicillin (DMEM-C).

Normal brain primary cultures

Murine brain primary cultures (NBPC-GFP) were generated from C57BL/6- Tg (ACTbEGFP)10sb/J transgenic mice expressing the enhanced green fluorescent reporter protein under the chicken β-actin gene promoter, kindly provided by Dr. Campetella. Animal procedures followed the guidelines from our Laboratory Animal Welfare Committee CICUAL—Facultad de Farmacia y Bioquímica—Universidad de Buenos Aires (RES (D) N° 4538/2018). Tissue manipulation and culture procedures were adapted from methods optimized for rat brain cultures (Carden et al., 2019; Pérez et al., 2013). Briefly, 2–4-day-old mice were euthanized by decapitation and brains were resected. Meninges were removed, and cerebral hemispheres were mechanically dissociated in DMEM/F12 medium. The largest tissue fragments were allowed to spontaneously settle, while the upper homogenous cell suspension was recovered and centrifuged. The pellet was resuspended in 1 mL of DMEM/F12 supplemented with 10% FBS. Finally, cells were cultured on either poly-lysine-coated coverslips or 12 well plates at 37°C in a 5% CO_2 atmosphere in fresh DMEM/F12 supplemented with 10% FBS, 20 µg/mL streptomycin and 20 IU/mL penicillin until cells reached confluence.

Neural stem cells (Neurospheres)

The subventricular zone was isolated from the brain of C57BL6-j mice and dissociated in DMEM-F12. The largest tissue fragments were allowed to spontaneously settle, while the upper homogenous cell suspension was recovered and centrifuged. The cellular pellet

was resuspended in DMEMF12, conditioned with the growth factors bFGF and EGF, and cultured at 37°C in a 5% CO_2 atmosphere. After a week, the formation of spherical structures was observed, namely neurospheres. These cultures are enriched in neural stem cells/progenitors, proliferate actively and could be differentiated to cells of all three neural lineages.

Coculture

The NBPC-GFP was grown to confluence in 12-well plates or 24-well plates containing coverslips. 3×10^5 or 1×10^5 GL26 cells, respectively, were then seeded onto the NBCP-GFP monolayer and incubated for 24 h. Subsequently, the coculture was treated with 4MU for 72 h and cell death was evaluated by flow cytometry using PI staining. For the immunofluorescence assay, the initial number of GL26 cells seeded was reduced respect to FC assay to facilitate the counting of each cell population. After incubation, the supernatant was removed, the cells were fixed with 4% paraformaldehyde (PFA) and the percentage of remnants GL26 (Vimentin-PE+) cells attached to the NBPC-GFP monolayer (GFP expressing cells) were evaluated.

Cell treatments

For all assays, cells were seeded 24 h before treatment. Cells were treated with either HA (0–300 µg/mL), TMZ (0–1000 µM) 4MU (0–1000 µM) or appropriate combinations. Untreated and vehicle control medium were also included. All incubations were performed at 37°C in a 5% CO_2 atmosphere.

HA was prepared in phosphate buffer saline (PBS). 4MU was dissolved (22.2 mg/ml) in methanol (Meth) and culture medium was added to reach a final concentration. TMZ was dissolved directly in culture medium.

XTT assay

For the XTT assay, 5×10^3 cells/well were seeded in 96-well plates and treated with 4MU, TMZ and/or HA for 48 h. After treatment, 25 µL of an XTT solution (1 mg/ml) containing PMS (7.5 µg/mL) were added to the culture medium (100 µL) and cells were incubated for two additional hours at 37°C in a 5% CO_2 atmosphere. After incubation, the absorbance (Abs) was read at 450 nm and 620 nm using a microplate reader (Multiscan Ex, Absorbance Microplate Reader, Thermo Electron Corporation, China). Cell viability was calculated as follows:

$$\text{Absorbance related to basal (\%)} = \frac{\text{Abs}(\text{treated}_{450\text{ nm}} - \text{Abs}(\text{treated}_{620\text{ nm}})}{\text{Abs}(\text{untreated}_{450\text{ nm}} - \text{Abs}(\text{untreated}_{620\text{ nm}})} \times 100$$

Proliferation

Cell proliferation was determined by BrdU incorporation assay and IFI. Briefly, 1.5×10^3 cells/well were seeded in 24-well plates on coverslips and treated by 47.5 h with 4MU. Then, BrdU was added at final concertation of 10 µM and cell were incubated for 30 min. After this time, the supernatant was removed, the cells were fixed with PFA 4% by 20 min and permeabilized with HCl 2N. Then, the cells were neutralized with sodium tetraborate (0.1 M; pH = 9), blocked with SFB 2% for 4 h and incubated with the mouse anti-BrdU antibody O.N. at 4°C. Finally, the antimouse secondary antibody was added plus DAPI (1 µg/mL) and incubated by 2 h. The coverslips were mounted with Mowiol and observed at fluorescence microscopy.

The proliferation was calculated as follows:

$$[\text{BrdU positive nuclei/total of nucleus}] \times 100$$

Cell death

Propidium iodide staining was performed as previously described (Lompardía et al., 2013, 2016; Papademetrio et al., 2014, 2016). Briefly, 3×10^5 cells/well were seeded in 12-well plates and treated for 72 h. Cells were then stained with FDA (1.4 µM) for 20 min, harvested, centrifuged and washed. Subsequently, the cell pellet was resuspended and incubated with PI (5 µg/mL) for 5 min. Stained cells were acquired on a Pas III flow cytometer (FC) (Partec, Germany) and analyzed with the Flowing 2.1.5 software (Scripps Institute, La Jolla, USA).

Evaluation of apoptosis

Apoptosis was evaluated by membrane asymmetry and DNA fragmentation assays. Briefly, after treating cultures for 72 h, cells were harvested, centrifuged and washed. Subsequently, membrane asymmetry was evaluated with the Annexin-V-PE Apoptosis Detection Kit I (BD Biosciences, USA) following the manufacturer's instructions. A Pas III flow cytometer (Partec, Germany) was used to acquire data that was analyzed with the flowing 2.5 software (Scripps Institute, La Jolla, USA). For DNA fragmentation, cells were harvested, centrifuged, washed and fixed with 2% PFA in PBS, stained with DAPI (1 µg/mL) and evaluated by fluorescence microscopy (Olympus BX51, Olympus America Inc.) (Cavaliere et al., 2009; Papademetrio et al., 2014).

Zymography

The MMPs activity was evaluated by gelatin zymography as previously described (Alaniz et al., 2004; Bencsik et al., 2017). Briefly, 2×10^5 cells/well were incubated in 48-well plates with serum-free DMEM supplemented with 0.01% BSA and 0.1% glucose with or without each treatment. After 24 h, supernatants were centrifuged and loaded on 7.5% SDS-PAGE gels containing gelatin (1 mg/mL). A molecular weight marker was run simultaneously. After electrophoresis, gels were washed three times with 2.5% Triton X-100 for 20 min, and then incubated with 25 mM Tris-HCl pH7.5; 5 mM $CaCl_2$; 0.9% NaCl; 0.05% NaN_3 for 48 h at 37°C. The gelatinolytic activity was revealed by staining with 0.5% Coomassie blue. Photographs were obtained with a BioSpectrum® 515 Imaging System M-26XV (UVP, Cambridge, UK) and analyzed with the Scion Image Software (Scion Corporation).

Wound-healing assay

Migration assay was performed as previously described, with slight modifications (Mascaró et al., 2017). Cells were seeded in 24-well plates until reaching confluence. The monolayer was then scratched with a 200 µL sterile pipette tip and incubated in DMEM containing 3% SFB with or without each treatment. The same wound area was photographed at 0, 6 and 18 h. The Image J software was used to calculate wound area.

Results were expressed as migration index calculated as follows:

$$\text{Closure gap index} = \frac{[(\text{area}_{t=0h}) - (\text{area}_{t=18h})]_{\text{treated}}}{[(\text{area}_{t=0h}) - (\text{area}_{t=18h})]_{\text{untreated}}}$$

Measurement of HA levels by enzyme-linked immunosorbent assay (ELISA)

HA levels in cell supernatant were measured by a competitive ELISA as described previously (Cordo Russo et al., 2012). Briefly, 96 well microtiter plates were coated with 100 µg/mL HMW-HA at 4°C. Samples and standard HMW-HA were incubated with 0.75 µg/mL bHABP at 37°C. The plate was blocked and incubated with the samples at 37°C for 4 h. After washing, the bHABP bound was determined using an avidin–HRP detection system. Sample concentrations were calculated from a standard curve.

Indirect immunofluorescence

After each treatment, cells were fixed with 4% PFA in PBS for 15 min, washed and blocked with PBS containing 5% SFB and 0.1% TritonX-100 for 2 h. Cells were then incubated in 1% FBS overnight at 4°C with the following primary antibodies: anti-CD44, anti-RHAMM, V9 antivimentin, anti-Sox10, anti-PFGFRα and anti-MBP, or with HABPb for HA staining followed by antimouse the correspondent secondary antibody, or streptavindin-cy2 for HA staining and 5 µg/mL Höechst dye. After washing, cells were mounted with Mowiol mounting medium on glass slides and micrographs were obtained by an Olympus BX51 microscope equipped with an Olympus DP73 camera (Olympus America Inc.) Images were analyzed with the Image Pro Plus 5.1 software (media Cybernetics).

Statistical analysis

Results were analyzed by one way-ANOVA follower by either the Bonferroni's or the Dunnet's posttests, or by two way-ANOVA followed by the Sidkay's posttest as required. The analysis was performed using the Prism software 6.0 (Graph Pad, San Diego, CA, USA). P-values < 0.05 were considered statistically significant. The drug combination analysis was performed according to the Bliss independence model (Foucquier and Guedj, 2015).

Supplementary data

Supplementary data is available at *Glycobiology* online.

Availability of data and materials

The datasets used and/or analyzed during the current study are available from the corresponding author on reasonable request.

Authors contributions

Matías A. Pibuel performed most of the experiments, contributed to the design of the study, analyzed the data and wrote the manuscript. Mariángeles Díaz performed cell death experiments and edited the manuscript. Yamila Molinari contributed to the design of the study, editing and supervision of the manuscript. Daniela Poodts prepared figures and edited the manuscript. Lucas Silvestroff collaborated editing manuscript. Silvina L. Lompardía and Paula Franco contributed equally to the realization of this work. Both contributed to the design of the study. Silvia E Hajos is the director of the group and supervised the work. All authors contributed to the work and have read and approved the final manuscript.

Acknowledgements

We are grateful to Susana Costantino, PhD and Lombardo Tomás, PhD for their technical assistance. We thank to LKM laboratories (Argentina) for providing temozolomide and Farmatrade Argentina for providing hyaluronan.

Funding

This work was supported by Consejo Nacional de Investigaciones Científicas y Técnicas: CONICET, [PIP No. 0428] to Dr. Álvarez and HS and [PIP 0289] to PF; by Universidad de Buenos Aires [UBACYT 20020170100454BA] to HS and LS and [UBACYT 20020150100091BA] to PF; and by Agencia Nacional de Promoción Científica y Tecnológica, [PICT-2017-2971] to SL.

Conflict of interest statement

None declared.

List of Abbreviations

4MU, 4-Methylumbelliferone; bHABP, biotinylated Hyaluronic Acid Binding Protein; CNS, Central nervous system; DAPI, 4′,6-diamidino-2-phenylindole; ECM, Extracellular matrix; FBS, Fetal bovine serum; FDA, Fluorescein diacetate; GAG, Glycosaminoglycan; GBM, Glioblastoma; GFP, Green fluorescent protein; HA, Hyaluronic acid; HAS, hyaluronic acid synthase; HMW, High molecular weight; Hyal, Hyaluronidase; LMW, Low molecular weight; Meth, Methanol; MMP, Metalloproteinase; NBPC, Murine normal brain primary cultures; NBPC-GFP, murine normal brain primary cultures expressing the green fluorescent protein; PBS, phosphate buffer saline; PE, Phycoerythrin; PFA, paraformaldehyde; PI, Propidium iodide; PMS, Phenazine methosulfate; RHAMM, Receptor for HA-mediated motility; TMZ, Temozolomide; XTT, (sodium 2,3,-bis(2-methoxy-4-nitro-5-sulfophenyl)-5-[(phenylamino)-carbonyl]-2H-tetrazolium) inner salt

References

Alaniz L, García M, Cabrera P, Arnaiz M, Cavaliere V, Blanco G, Alvarez E, Hajos S. 2004. Modulation of matrix metalloproteinase-9 activity by hyaluronan is dependent on NF-κB activity in lymphoma cell lines with dissimilar invasive behavior. *Biochem Biophys Res Commun*. 324(2):736–743. doi: 10.1016/j.bbrc.2004.09.120.

Anjum K, Shagufta BI, Abbas SQ, Patel S, Khan I, Shah SAA, Akhter N, UI Hassan SS. 2017. Current status and future therapeutic perspectives of glioblastoma multiforme (GBM) therapy: A review. *Biomed Pharmacother*. 92:681–689. doi: 10.1016/j.biopha.2017.05.125.

Anton K, Baehring JM, Mayer T. 2012. Glioblastoma multiforme: Overview of current treatment and future perspectives. *Hematol Oncol Clin North Am*. 26(4):825–853. doi: 10.1016/j.hoc.2012.04.006.

Arai E, Nishida Y, Wasa J, Urakawa H, Zhuo L, Kimata K, Kozawa E, Futamura N, Ishiguro N. 2011. Inhibition of hyaluronan retention by 4-methylumbelliferone suppresses osteosarcoma cells in vitro and lung metastasis in vivo. *Br J Cancer*. 105(12):1839–1849. doi: 10.1038/bjc.2011.459.

Auvinen P, Tammi R, Kosma VM, Sironen R, Soini Y, Mannermaa A, Tumelius R, Uljas E, Tammi M. 2013. Increased hyaluronan content and stromal cell CD44 associate with HER2 positivity and poor prognosis in human breast cancer. *Int J Cancer*. 132(3):531–539. doi: 10.1002/ijc.27707.

Bencsik P, Bartekova M, Görbe A, Kiss K, Pálóczi J, Radosinska J, Szűcs G, Ferdinandy P (2017). MMP activity detection in zymograms. In *Methods in Molecular Biology* (Vol. 1626), Totowa, NJ: Humana Press Inc, pp. 53–70.

Boregowda RK, Appaiah HN, Siddaiah M, Kumarswamy SB, Sunila S, Thimmaiah KN, Mortha KK, Toole B, Banerjee SD. 2006. Expression of hyaluronan in human tumor progression. *J Carcinog*. 5:1–19. doi: 10.1186/1477-3163-5-2.

Brunetti A, Marinelli O, Morelli MB, Iannarelli R, Amantini C, Russotti D, Santoni G, Maggi F, Nabissi M. 2019. Isofuranodiene synergizes with temozolomide in inducing glioma cells death. *Phytomedicine*. 52:51–59. doi: 10.1016/j.phymed.2018.09.220.

Carden TR, Correale J, Pasquini JM, Pérez MJ. 2019. Transferrin enhances microglial phagocytic capacity. *Mol Neurobiol*. 56(9):6324–6340. doi: 10.1007/s12035-019-1519-0.

Cavaliere V, Papademetrio DL, Lorenzetti M, Valva P, Preciado MV, Gargallo P, Larripa I, Monreal MB, Pardo ML, Hajos SE, et al. 2009. Caffeic acid Phenylethyl Ester and MG-132 have apoptotic and Antiproliferative effects on leukemic cells but not on normal mononuclear cells. *Transl Oncol*. 2(1):46–58. doi: 10.1593/tlo.08202.

Chaudhary AK, Chaudhary S, Ghosh K, Nadkarni A. 2016. Pleiotropic roles of metalloproteinases in hematological malignancies: An update. *Asian Pac J Cancer Prev*. 17(7):3043–3051. http://www.ncbi.nlm.nih.gov/pubmed/27509927.

Chetty C, Vanamala SK, Gondi CS, Dinh DH, Gujrati M, Rao JS. 2012. MMP-9 induces CD44 cleavage and CD44 mediated cell migration in glioblastoma xenograft cells. *Cell Signal*. 24(2):549–559. doi: 10.1016/j.cellsig.2011.10.008.

Chintala SK, Tonn JC, Rao JS. 1999. Matrix metalloproteinases and their biological function in human gliomas. *Int J Dev Neurosci*. 17:495–502.

Cho H, Matsumoto S, Fujita Y, Kuroda A, Menju T, Sonobe M, Kondo N, Torii I, Nakano T, Lara PN, et al. 2017. Trametinib plus 4-Methylumbelliferone exhibits antitumor effects by ERK blockade and CD44 downregulation and affects PD-1 and PD-L1 in malignant pleural mesothelioma. *J Thorac Oncol*. 12(3):477–490. doi: 10.1016/j.jtho.2016.10.023.

Cordo Russo RI, Ernst G, Lompardía S, Blanco G, Álvarez É, Garcia MG, Hajos S. 2012. Increased hyaluronan levels and decreased dendritic cell activation are associated with tumor invasion in murine lymphoma cell lines. *Immunobiology*. 217(9):842–850. doi: 10.1016/j.imbio.2011.12.006.

Csoka AB, Stern R. 2013. Hypotheses on the evolution of hyaluronan: A highly ironic acid. *Glycobiology*. 23(4):398–411. doi: 10.1093/glycob/cws218.

Delpech B, Maingonnat C, Girard N, Chauzy C, Olivier A, Maunoury R, Tayot J, Creissard P. 1993. Hyaluronan and hyaluronectin in the extracellular matrix of human brain tumour stroma. *Eur J Cancer*. 29(7):1012–1017. doi: 10.1016/S0959-8049(05)80214-X.

DeSouza LV, Matta A, Karim Z, Mukherjee J, Wang XS, Krakovska O, Zadeh G, Guha A, Siu KWM. 2013. Role of moesin in hyaluronan induced cell migration in glioblastoma multiforme. *Mol Cancer*. 12(1):74. doi: 10.1186/1476-4598-12-74.

Ferrer VP, Moura Neto V, Mentlein R. 2018. Glioma infiltration and extracellular matrix: Key players and modulators. *Glia*. (January):1542–1565. doi: 10.1002/glia.23309.

Foucquier J, Guedj M. 2015. Analysis of drug combinations: Current methodological landscape. *Pharmacol Res Perspect*. 3(3). doi: 10.1002/prp2.149.

Hascall VC, Wang A, Tammi M, Oikari S, Tammi R, Passi A, Vigetti D, Hanson RW, Hart GW. 2014. The dynamic metabolism of hyaluronan regulates the cytosolic concentration of UDP-GlcNAc. *Matrix Biol*. 35:14–17. doi: 10.1016/j.matbio.2014.01.014.

Houy N, Le Grand F. 2018. Administration of temozolomide: Comparison of conventional and metronomic chemotherapy regimens. *J Theor Biol*. 446:71–78. doi: 10.1016/j.jtbi.2018.02.034.

Ishizuka S, Askew EB, Ishizuka N, Knudson CB, Knudson W. 2016. 4-Methylumbelliferone diminishes catabolically activated articular chondrocytes and cartilage explants via a mechanism independent of hyaluronan inhibition. *J Biol Chem*. 291(23):12087–12104. doi: 10.1074/jbc.M115.709683.

Jiang D, Liang J, Noble PW. 2011. Hyaluronan as an immune regulator in human diseases. *Physiol Rev*. 91(1):221–264. doi: 10.1152/physrev.00052.2009.

Jin SG, Jeong YI, Jung S, Ryu HH, Jin YH, Kim IY. 2009. The effect of hyaluronic acid on the invasiveness of malignant glioma cells: Comparison of invasion potential at hyaluronic acid hydrogel and Matrigel. *J Korean Neurosurg Soc*. 46(5):472–478. doi: 10.3340/jkns.2009.46.5.472.

Joy RA, Vikkath N, Ariyannur PS. 2018. Metabolism and mechanisms of action of hyaluronan in human biology. *Drug Metab Pers Ther*. 33(1):15–32. doi: 10.1515/dmpt-2017-0031.

Junker N, Latini S, Petersen LN, Kristjansen PEG. 2003. Expression and regulation patterns of hyaluronidases in small cell lung cancer and glioma lines. *Oncol Rep*. 10(3):609–616.

Kakizaki I, Kojima K, Takagaki K, Endo M, Kannagi R, Ito M, Maruo Y, Sato H, Yasuda T, Mita S, et al. 2004. A novel mechanism for the inhibition of hyaluronan biosynthesis by 4-methylumbelliferone. *J Biol Chem*. 279(32):33281–33289. doi: 10.1074/jbc.M405918200.

Karalis T, Heldin P, Vynios D, Neill T, Buraschi S, Iozzo R, Karamanos NK, Skandalis S. 2019. Tumor-suppressive functions of 4-MU on breast cancer cells of different ER status: Regulation of hyaluronan/HAS2/CD44 and specific matrix effectors. *Matrix Biol*. 78–79:118–138. doi: 10.1016/j.matbio.2018.04.007.

Kast RE, Halatsch M. 2012. Matrix Metalloproteinase-2 and -9 in glioblastoma: A trio of old drugs — Captopril, disulfiram and nelfinavir—Are inhibitors with potential as adjunctive treatments in glioblastoma. *Arch Med Res*. 43(3):243–247. doi: 10.1016/j.arcmed.2012.04.005.

Khaldoyanidi SK, Goncharova V, Mueller B, Schraufstatter IU. 2014. Hyaluronan in the healthy and malignant hematopoietic microenvironment. *Adv Cancer Res*. 123:149–189. doi: 10.1016/B978-0-12-800092-2.00006-X.

Kultti A, Pasonen-Seppänen S, Jauhiainen M, Rilla KJ, Kärnä R, Pyöriä E, Tammi RH, Tammi MI. 2009. 4-Methylumbelliferone inhibits hyaluronan synthesis by depletion of cellular UDP-glucuronic acid and downregulation of hyaluronan synthase 2 and 3. *Exp Cell Res*. 315(11):1914–1923. doi: 10.1016/j.yexcr.2009.03.002.

Lokeshwar VB, Lopez LE, Munoz D, Chi A, Shirodkar SP, Lokeshwar SD, Escudero DO, Dhir N, Altman N. 2010. Antitumor activity of hyaluronic acid synthesis inhibitor 4-methylumbelliferone in prostate cancer cells. *Cancer Res*. 70(7):2613–2623. doi: 10.1158/0008-5472.CAN-09-3185.

Lompardía SL, Díaz M, Papademetrio DL, Mascaró M, Pibuel M, Álvarez E, Hajos SE. 2016. Hyaluronan oligomers sensitize chronic myeloid leukemia cell lines to the effect of Imatinib. *Glycobiology*. 26(4):343–352. http://glycob.oxfordjournals.org/content/26/4/343.abstract.

Lompardía SL, Díaz M, Papademetrio DL, Pibuel M, Álvarez É, Hajos SE. 2017. 4-methylumbelliferone and imatinib combination enhances senescence induction in chronic myeloid leukemia cell lines. *Invest New Drugs*. 35(1):1–10. doi: 10.1007/s10637-016-0397-9.

Lompardía SL, Papademetrio DL, Mascaró M, Del Carmen Álvarez EM, Hajos SE. 2013. Human leukemic cell lines synthesize hyaluronan to avoid senescence and resist chemotherapy. *Glycobiology*. 23(12):1463–1476. doi: 10.1093/glycob/cwt074.

Louis DN, Perry A, Reifenberger G, von Deimling A, Figarella-Branger D, Cavenee WK, Ohgaki H, Wiestler OD, Kleihues P, Ellison DW. 2016. The 2016 World Health Organization classification of tumors of the central nervous system: A summary. *Acta Neuropathol*. 131(6):803–820. doi: 10.1007/s00401-016-1545-1.

Mascaró M, Pibuel MA, Lompardía SL, Díaz M, Zotta E, Bianconi MI, Lago N, Otero S, Jankilevich G, Alvarez E, et al. 2017. Low molecular weight hyaluronan induces migration of human choriocarcinoma JEG-3 cells mediated by RHAMM as well as by PI3K and MAPK pathways. *Histochem Cell Biol*. 148(2). doi: 10.1007/s00418-017-1559-3.

Maxwell CA, McCarthy J, Turley E. 2008. Cell-surface and mitotic-spindle RHAMM: Moonlighting or dual oncogenic functions? *J Cell Sci*. 121(Pt 7):925–932. doi: 10.1242/jcs.022038.

Mooney KL, Choy W, Sidhu S, Pelargos P, Bui TT, Voth B, Barnette N, Yang I. 2016. The role of CD44 in glioblastoma multiforme. *J Clin Neurosci*. 34:1–5. doi: 10.1016/j.jocn.2016.05.012.

Morera DS, Hennig MS, Talukder A, Lokeshwar SD, Wang J, Garcia-roig M, Ortiz N, Yates TJ, Lopez LE, Kallifatidis G, et al. 2017. Hyaluronic acid family in bladder cancer: Potential prognostic biomarkers and therapeutic targets. 117(10):1507–1517. doi: 10.1038/bjc.2017.318.

Musumeci G, Magro G, Cardile V, Coco M, Marzagalli R, Castrogiovanni P, Imbesi R, Eleonora Graziano AC, Barone F, Di Rosa M, et al. 2015. Characterization of matrix metalloproteinase-2 and -9, ADAM-10 and N-cadherin expression in human glioblastoma multiforme. *Cell Tissue Res*. 362(1):45–60. doi: 10.1007/s00441-015-2197-5.

Nagy N, Gurevich I, Kuipers HF, Ruppert SM, Marshall PL, Xie BJ, Sun W, Malkovskiy AV, Rajadas J, Grandoch M, et al. 2019. 4-Methylumbelliferyl glucuronide contributes to hyaluronan synthesis inhibition. *J Biol Chem*. 294(19):7864–7877. doi: 10.1074/jbc.RA118.006166.

Nagy N, Kuipers HF, Frymoyer AR, Ishak HD, Bollyky JB, Wight TN, Bollyky PL. 2015. 4-Methylumbelliferone treatment and hyaluronan inhibition as a therapeutic strategy in inflammation, autoimmunity, and cancer. *Front Immunol*. 6(MAR):123. doi: 10.3389/fimmu.2015.00123.

Nakada M, Okada Y, Yamashita J. 2003. The role of matrix metalloproteinases in glioma invasion. *Front Biosci*. 8:261–269.

Navone SE, Guarnaccia L, Cordiglieri C, Crisà FM, Caroli M, Locatelli M, Schisano L, Rampini P, Miozzo M, Verde NL, et al. 2018. Aspirin affects tumor angiogenesis and sensitizes human glioblastoma endothelial cells to Temozolomide, bevacizumab, and Sunitinib, impairing vascular endothelial growth factor-related signaling. *World Neurosurg*. 120:380–391. doi: 10.1016/j.wneu.2018.08.080.

Novak U, Stylli SS, Kaye AH, Lepperdinger G. 1999. Hyaluronidase-2 overexpression accelerates intracerebral but not subcutaneous tumor formation of murine astrocytoma cells. *Cancer Res*. 59(24): 6246–6250.

Papademetrio DL, Cavaliere V, Simunovich T, Costantino S, Campos MD, Lombardo T, Kaiser CMF, Álvarez É. 2014. Interplay between autophagy and apoptosis in pancreatic tumors in response to gemcitabine. *Target Oncol*. 9(2):123–134. doi: 10.1007/s11523-013-0278-5.

Papademetrio DL, Lompardía SL, Simunovich T, Costantino S, Mihalez CY, Cavaliere V, Álvarez É. 2016. Inhibition of survival pathways MAPK and NF-kB triggers apoptosis in pancreatic ductal adenocarcinoma cells via suppression of autophagy. *Target Oncol*. 11(2):183–195. doi: 10.1007/s11523-015-0388-3.

Park JB, Kwak HJ, Lee SH. 2008. Role of hyaluronan in glioma invasion. *Cell Adh Migr*. 2(3):202–207. doi: 10.4161/cam.2.3.6320.

Park JH, Ryu CH, Kim MJ, Jeun SS. 2015. Combination therapy for gliomas using temozolomide and interferon-beta secreting human bone marrow derived mesenchymal stem cells. *J Korean Neurosurg Soc*. 57(5):323–328. doi: 10.3340/jkns.2015.57.5.323.

Pérez MJ, Fernandez N, Pasquini JM. 2013. Oligodendrocyte differentiation and signaling after transferrin internalization: A mechanism of action. *Exp Neurol*. 248:262–274. doi: 10.1016/j.expneurol.2013.06.014.

Piccioni F, Malvicini M, Garcia MG, Rodriguez A, Atorrasagasti C, Kippes N, Piedra Buena IT, Rizzo MM, Bayo J, Aquino J, et al. 2012. Antitumor effects of hyaluronic acid inhibitor 4-methylumbelliferone in an orthotopic hepatocellular carcinoma model in mice. *Glycobiology*. 22(3):400–410. doi: 10.1093/glycob/cwr158.

Preston M, Sherman LS. 2011. Neural stem cell niches: Roles for the hyaluronan-based extracellular matrix. *Front Biosci (Schol Ed)*. 3:1165–1179. doi: 10.2741/218.

Provenzano PP, Hingorani SR. 2013. Hyaluronan, fluid pressure, and stromal resistance in pancreas cancer. *Br J Cancer*. 108(1):1–8. doi: 10.1038/bjc.2012.569.

Przystal JM, Hajji N, Khozoie C, Renziehausen A, Zeng Q, Abaitua F, Hajitou A, Suwan K, Want E, Bomalaski J, et al. 2018. Efficacy of arginine depletion by ADI-PEG20 in an intracranial model of GBM. *Cell Death Dis*. 9(12). doi: 10.1038/s41419-018-1195-4.

Sasmita AO, Wong YP, Ling APK. 2018. Biomarkers and therapeutic advances in glioblastoma multiforme. *Asia Pac J Clin Oncol*. 14(1):40–51. doi: 10.1111/ajco.12756.

Sironen RK, Tammi M, Tammi R, Auvinen PK, Anttila M, Kosma VM. 2011. Hyaluronan in human malignancies. *Exp Cell Res*. 317(4):383–391. doi: 10.1016/j.yexcr.2010.11.017.

Su W, Matsumoto S, Sorg B, Sherman LS. 2019. Distinct roles for hyaluronan in neural stem cell niches and perineuronal nets. *Matrix Biol*. 78–79(2017):272–283. doi: 10.1016/j.matbio.2018.01.022.

Termeer C, Sleeman JP, Simon JC. 2003. Hyaluronan - magic glue for the regulation of the immune response? *Trends Immunol*. 24(3):112–114. doi: 10.1016/S1471-4906(03)00029-2.

Toole BP. 2004. Hyaluronan: From extracellular glue to pericellular cue. *Nat. Rev. Cancer*. 4(7):528–539. doi: 10.1038/nrc1391.

Toole BP. 2009. Hyaluronan-CD44 interactions in cancer: Paradoxes and possibilities. *Clin Cancer Res*. 15(24):7462–7468. doi: 10.1158/1078-0432.CCR-09-0479.Hyaluronan-CD44.

Tsatas D, Kanagasundaram V, Kaye A, Novak U. 2002. EGF receptor modifies cellular responses to hyaluronan in glioblastoma cell lines. *J Clin Neurosci*. 9(3):282–288. doi: 10.1054/jocn.2001.1063.

Urakawa H, Nishida Y, Wasa J, Arai E, Zhuo L, Kimata K, Kozawa E, Futamura N, Ishiguro N. 2012. Inhibition of hyaluronan synthesis in breast cancer cells by 4-methylumbelliferone suppresses tumorigenicity in vitro and metastatic lesions of bone in vivo. *Int J Cancer*. 130(2):454–466. doi: 10.1002/ijc.26014.

Varga I, Hutóczki G, Petrás M, Scholtz B, Mikó E, Kenyeres A, Tóth J, Zahuczky G, Bognár L, Hanzély Z, et al. 2010. Expression of invasion-related extracellular matrix molecules in human glioblastoma versus intracerebral lung adenocarcinoma metastasis. *Zentralblatt Fur Neurochirurgie*. 71(4):173–180. doi: 10.1055/s-0030-1249698.

Vigetti D, Rizzi M, Moretto P, Deleonibus S, Dreyfuss JM, Karousou E, Viola M, Clerici M, Hascall VC, Ramoni MF, et al. 2011. Glycosaminoglycans and glucose prevent apoptosis in 4-methylumbelliferone-treated human aortic smooth muscle cells. *J Biol Chem*. 286(40):34497–34503. doi: 10.1074/jbc.M111.266312.

Zheng Y, Miu Y, Yang X, Yang X, Zhu M. 2017. CCR7 mediates TGF-β1-induced human malignant glioma invasion, migration, and epithelial–mesenchymal transition by activating MMP2/9 through the nuclear factor KappaB signaling pathway. *DNA Cell Biol*. 36(10):853–861. doi: 10.1089/dna.2017.3818.